**Supporting information**

# Revealing the Gas Sensitive Stability of Formate Species during $CO_2$ Hydrogenation

Didi Li[1], Shiqing Jin[1], Zhen Wang[1], Zhaocong Jiang[1], Feng Xiong[2], Jianqiang Wang[2], Minghui Zhu[1*]

[1] State Key Laboratory of Chemical Engineering, East China University of Science and Technology, 130 Meilong Road, Shanghai 200237, China

[2] Sinopec Shanghai Research Institute of Petrochemical Technology, 1658 Pudong Beilu, Shanghai 201208, China.

* Corresponding E-mail: minghuizhu@ecust.edu.cn

**Catalyst preparation.** The $CuO/CeO_2$ and $CuO/Al_2O_3$ were prepared with a deposition-precipitation method using $CeO_2$ and $Al_2O_3$ as the catalyst support. First, support (2 g) was dispersed in deionized water (50 mL) under sonication to form a slurry. A solution of the desired amount of copper(II) nitrate trihydrate in 50 mL water was then added to the support–water mixture under sonication. Afterwards, the mixture was stirred under vigorous mechanical stirring. 1 g of $Na_2CO_3$ was dissolved in 50 mL deionized water and added to the solution mixture drowsily. The stirring was continued for 90 min before the solid product was collected by centrifugation (8000 rpm for 5 min). The product was then washed thoroughly with deionized water 4 times to remove the Na impurities. The solid precursor was dried at 90 °C overnight and then calcined at 450 °C (2 °C $min^{-1}$) for 3 h to obtain $CuO/CeO_2$ and $CuO/Al_2O_3$ samples.

The content of Cu was determined by inductively coupled plasma optical emission spectrometry (Agilent 725ES).

***Operando* DRIFTS-MS measurements.** A PerkinElmer FT-IR spectrometer was adopted to carry out *in situ* DRIFTS analysis. The measurements were performed in a low void-volume cell (DR-A01, Jiaxing Puxiang Tech. Ltd.). The samples were first reduced under a 10%$H_2$/Ar gas mixture of 50 mL $min^{-1}$ for 1 h at 300 °C and then cooled down in Ar to target temperature. Afterward, the 45%$CO_2$/45%$H_2$/Ar (50 mL $min^{-1}$) gas mixture was introduced for 40 min and subsequently switched to a 10%$H_2$/Ar or pure Ar (50 mL $min^{-1}$) for 20 min (Figure S2). A four-way switching valve was used to select the $CO_2$- or $H_2$-containing (or Ar) streams. The spectra were recorded every 6 s to follow the reaction and stabilization of the surface species. Finally, the gas effluents are analyzed online by mass spectrometry (MS). Signals of $H_2$ ($m/z = 2$), $H_2O$ ($m/z = 18$), CO ($m/z = 28$), $CO_2$ ($m/z = 44$), HCOOH ($m/z = 45$), and Ar ($m/z = 40$) were recorded with a MS. Note that the MS signal for CO was background-subtracted by $CO_2$ gas.

Continuous *in situ* DRIFTS experiment was employed during RWGS condition at different temperature using same catalyst. The samples were first reduced under a 10%$H_2$/Ar gas mixture of 50 mL $min^{-1}$ for 1 h at 300 °C and then cooled down in Ar to

200 °C. Afterward, the 45%$CO_2$/45%$H_2$/Ar (50 mL min$^{-1}$) gas mixture was introduced, and the DRIFTS were collected after the system reached balance. Then, as sequential increase temperature to 225 °C, 250 °C, 275 °C, and 300 °C, the spectra were recorded after the system reached balance at every temperature.

*In situ* DRIFTS after HCOOH or DCOOD adsorption experiment is as follows: the catalyst was reduced by 10%$H_2$/Ar and flushed with Ar, then exposed to a HCOOH/Ar or DCOOD/Ar mixture for 30 min at 110 °C. Afterwards, the inlet gas was switched to pure Ar with the spectra were recorded after the system reached balance.

***In situ* time-resolved Raman measurements.** *In situ* Raman spectra were collected with a Horiba LabRam-HR spectrometer equipped with a visible laser excitation at 514 nm generated by a He–Cd laser. The laser was focused on the sample with a confocal microscope equipped with a ×50 long working distance objective (Olympus BX-30-LWD). The scattered photons were directed and focused onto a single-stage monochromator measured with an ultraviolet-sensitive liquid-$N_2$-cooled CCD (charge-coupled device) detector (Horiba CCD-3000 V). The measurements were performed in a low void-volume cell (DR-A01, Jiaxing Puxiang Tech. Ltd.). The samples were first reduced under a 10%$H_2$/Ar gas mixture of 50 mL min$^{-1}$ for 1 h at 300 °C and then cooled down in Ar to target temperature. Afterward, the 45%$CO_2$/45%$H_2$/Ar (50 mL min$^{-1}$) gas mixture was introduced for 40 min and subsequently switched to a 10%$H_2$/Ar or pure Ar (50 mL min$^{-1}$) for 20 min, with the spectra collected every 10 s. A four-way switching valve was used to select the $CO_2$- or $H_2$-containing (or Ar) streams.

**Temperature-programmed with formic acid (HCOOH-TP) Measurements.** The HCOOH-TP experiments were conducted on the Cu/$CeO_2$ catalyst. The samples were first reduced under a 10%$H_2$/Ar gas mixture of 50 mL min$^{-1}$ for 1 h at 300 °C and then cooled down in Ar to 110 °C. Saturated HCOOH vapor was then introduced into the system by means of a 50 mL min$^{-1}$ Ar flow for 30 min from a bubbler that was maintained at 30 °C. After HCOOH adsorption, the system was further purged by Ar or 10%$H_2$/Ar flow until no signal of desorbed HCOOH ($m/z$ = 45) could be observed.

The test sample was then heated to 500 °C at a rate of 5 °C $min^{-1}$ under 50 mL $min^{-1}$ Ar flow. Signals of $H_2$ ($m/z = 2$), $H_2O$ ($m/z = 18$), CO ($m/z = 28$), $CO_2$ ($m/z = 44$), HCOOH ($m/z = 45$), and Ar ($m/z = 40$) were recorded with a MS. Note that the MS signal for CO was background-subtracted by $CO_2$ gas.

**Catalytic Testing**. The catalytic activity of the $Cu/CeO_2$ catalyst in the RWGS reaction was measured using a fixed-bed flow reactor (4 mm inner diameter) made of U-type quartz tube. The catalyst was sieved to the range of 60-80 mesh and then loaded into the reactor. Before being tested, the fresh catalyst was pretreated at 300 °C for 1 h using a feed that contained $10\%H_2/Ar$ to reduce and remove moisture from the sample. Then, the reaction mixture ($45\%CO_2/45\%H_2/Ar$) was introduced into the reactor with the high gas hourly space velocity (GHSV) to reach lower $CO_2$ conversion at different temperatures (from 200 to 300 °C) for 2 h for $Cu/CeO_2$. The gas chromatograph (Ruimin GC 2060, Shanghai) was equipped with both a thermal conductivity detector (TCD) and a flame ionization detector (FID). The TCD was used to quantify $N_2$, CO, $CO_2$, $H_2$, and the FID to quantify CO, $CO_2$, and $CH_4$. CO was the only observed product. Then $CO_2$ conversion ($X_{CO2}$) was concluded from the following:

$$X_{CO2}=([CO_2]_{inlet}-[CO_2]_{outlet})/[CO_2]_{inlet} \times 100\%$$

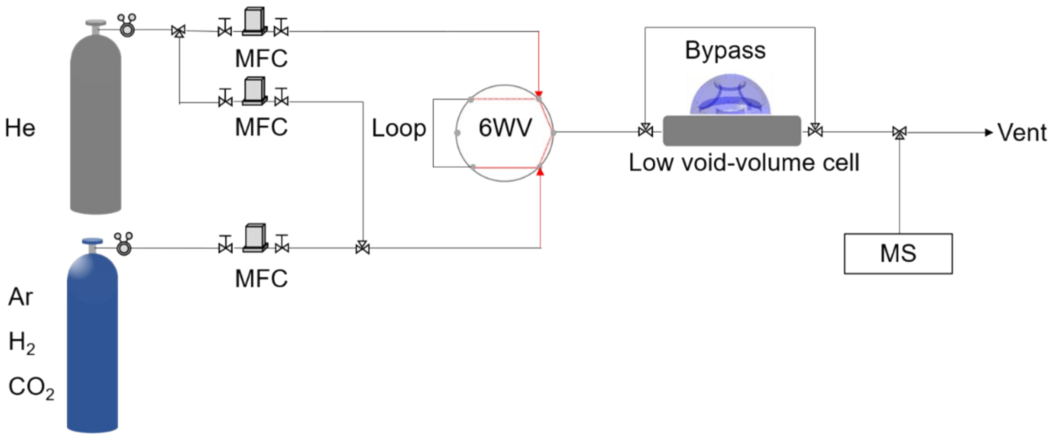

**Figure S1.** Schematics of the *in situ* low void-volume cell and experimental setup. MFC = mass flow controller; MS = mass spectrometer; 6WV = 6-port two-position switching valve. 6WV can switch to two positions (dotted and solid lines).

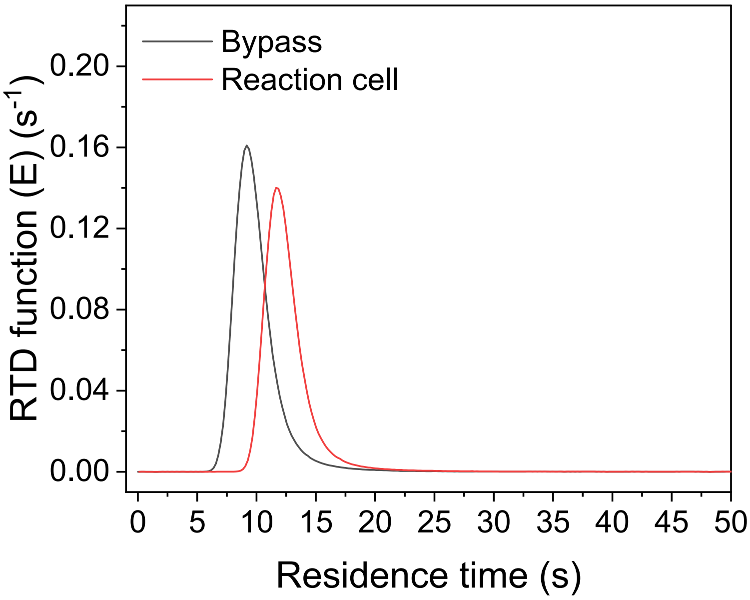

**Figure S2.** Residence time distribution (RTD) profiles of Ar gas pulse through the bypass and the reaction cell. Conditions: ambient temperature, 1 bar, 100 μL loop, He carrier flow of 50 mL/min.

Analysis of the cell's residence time distribution (RTD) was performed via a pulse technique. Briefly, RTD is measured with gas pulse injection experiments by monitoring the corresponding pulse gas concentration changes (C(t)) with residence time, *t*. The *C* vs. *t* data was normalized to give an area of 1 which defines the RTD or so-called E(t) curve.[1, 2] The reaction system is modified to provide a 100 μL sample loop in a 6-port two-position switching valve for pulse experiments with Ar, $CO_2$, and $H_2$ and He as the carrier gas. The lines from the point of the gas pulse injection (with a carrier flow rate of 50 mL min$^{-1}$) to the reaction cell and the MS were considered as a plug flow reactor (PFR) and continuously-stirred tank reactor (CSTR), respectively. In addition, the setup requires gas pulse measurements via a line that bypasses the reactor, which in combination with pulses through the reaction cell, allows estimation of the average residence time of the pulsed gases in the system components according to the references (Figure S3).[1, 2] A comparison of the normalized composition (*E*(*t*) function) of an Ar pulse through the bypass line with that one through the reaction cell (Figure S4) shows that they are similar in size, with the exception that the former is a bit sharper. This result indicates a minor contribution to the cell's RTD due to void volume. Results for the overall, *in situ* cell, and MS chamber's mean residence time (MRT) for different gases as well as the space time of transfer lines are shown in Table S2. At a gas flow rate of 50 mL min$^{-1}$, the average $t_{m,1}$ was 1.8 s, which suggests that the cell reported here can achieve rapid gas exchange (within about 1.5-2.0 s) at moderate gas flow rates (Table S2). Such rapid gas exchange ensures the rigorous implementation of continuous transient mode around a steady state to obtain kinetic spectral derived information.

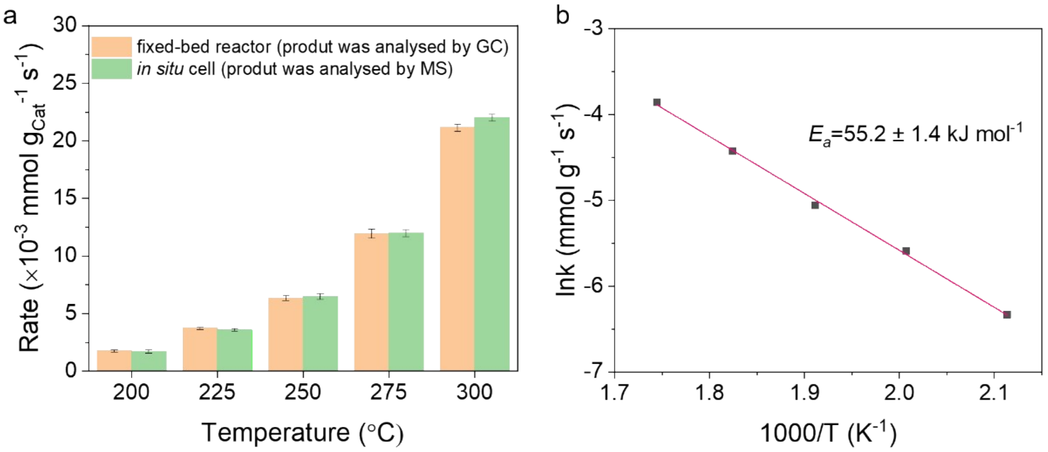

**Figure S3.** (a) Catalytic performance of the Cu/$CeO_2$ catalyst in the RWGS reaction within 200-300 °C. (b) Arrhenius plot for the Cu/$CeO_2$ catalyst in the RWGS reaction.

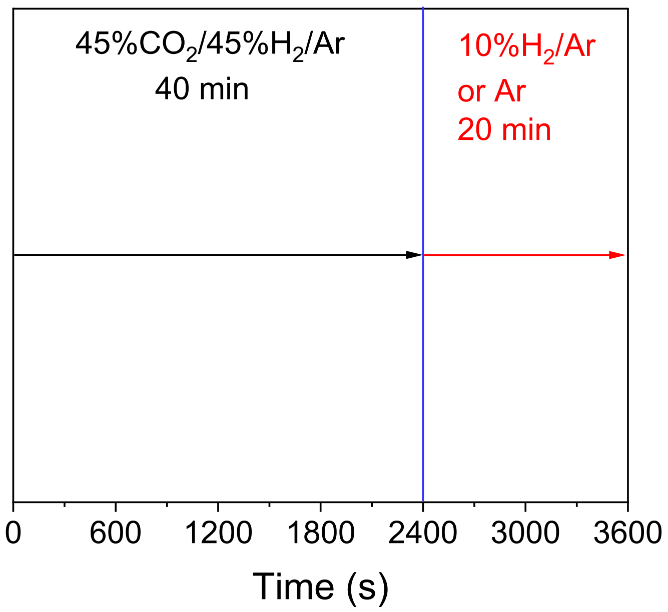

**Figure S4.** The schematic diagram for the procedure of the *in situ* time-resolved DRIFTS experiment.

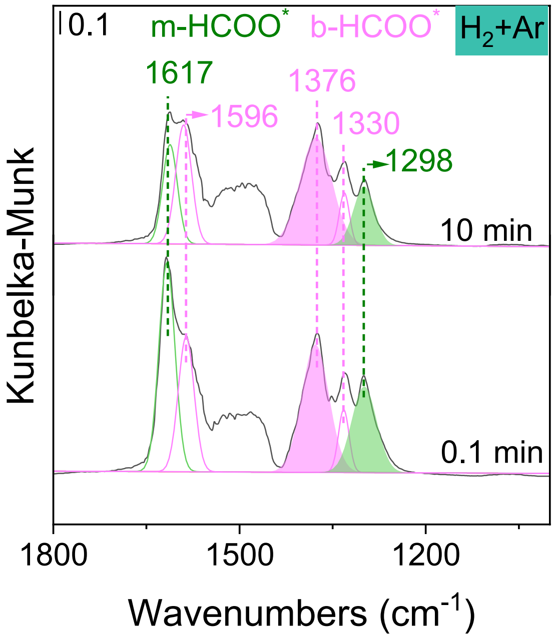

**Figure S5.** The representative figure shows the fitted curve, using a Gaussian curve fit, for *in situ* DRIFT spectra collected in 10%$H_2$/Ar with different time at 225 °C.

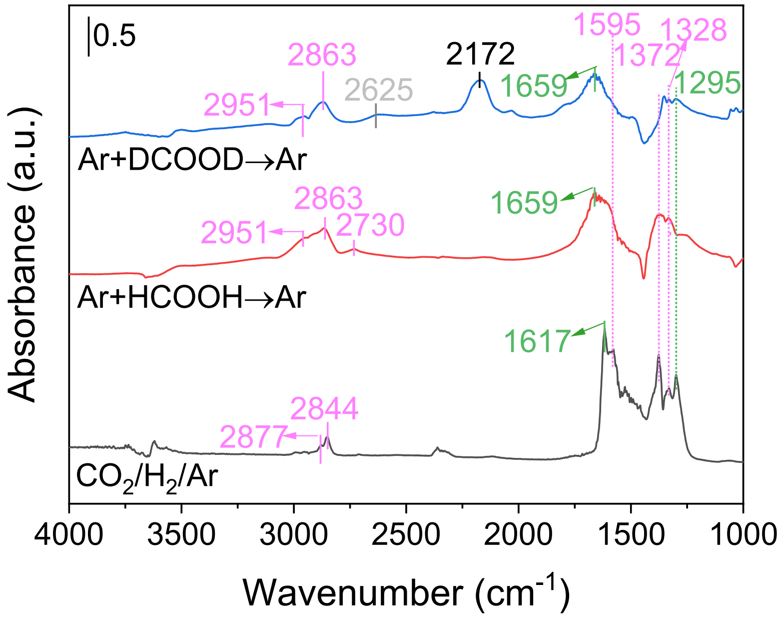

**Figure S6.** Comparison of steady DRIFT spectra recorded after switch from the Ar/HCOOH or Ar/DCOOD to Ar at 110 °C and in $CO_2/H_2/Ar$ flow at 200 °C.

*In situ* DRIFTS with HCOOH or DCOOD adsorption (HCOOH-DRIFTS or DCOOD-DRIFTS) was employed to gain insight into the correct assignments of the IR bands (Figure S6). The feature bands of formates consist of the bending vibration of the C-H bond (2700-3000 $cm^{-1}$) and stretching vibration modes (symmetric and asymmetric) of the O-C-O group (1200-1700 $cm^{-1}$). It is noted that the *in situ* HCOOH-DRIFTS show the feature bands of formates the same as spectra obtained during the flow of $CO_2/H_2$ mixture within 200-300 °C (Figure S6).

Then, we performed an extensive literature search that can help us confirm the assignments of absorption peaks (Table S3). Generally, the asymmetrical O-C-O bending of monodentate formate shows a higher wavenumber than that of bidentate formate, whereas the IR peak ascribed to the symmetrical O-C-O bending of monodentate formate has a lower wavenumber than that of bidentate formate. The *in situ* DCOOD-DRIFTS reveals that the bending vibration of the C-D band at 2172 $cm^{-1}$ and in-of-plane C-D bending at 1038 $cm^{-1}$ assigned to formates and out-of-plane OD bending (2625 $cm^{-1}$) are observed.[3, 4] However, there is no difference in the peak positions for the assignments of the O-C-O bending motion in 1200-1700 $cm^{-1}$ region because it do not involve H-D isotope exchange (Figure S6). Furthermore, two formate species showed different stability in 10%$H_2$/Ar, and the peaks at 1376 $cm^{-1}$ are still present at 300 °C (Figures R7-10). According to literature, the bidentate formate species are more stable than the monodentate formate species.[5, 6] Therefore, the above result also confirms that the correct assignment of IR peaks regarding both monodentate formate (1617, 1298, 2844 and 2877 $cm^{-1}$) and bidentate formate (1596, 1376, 1330, 2844 and 2877 $cm^{-1}$).

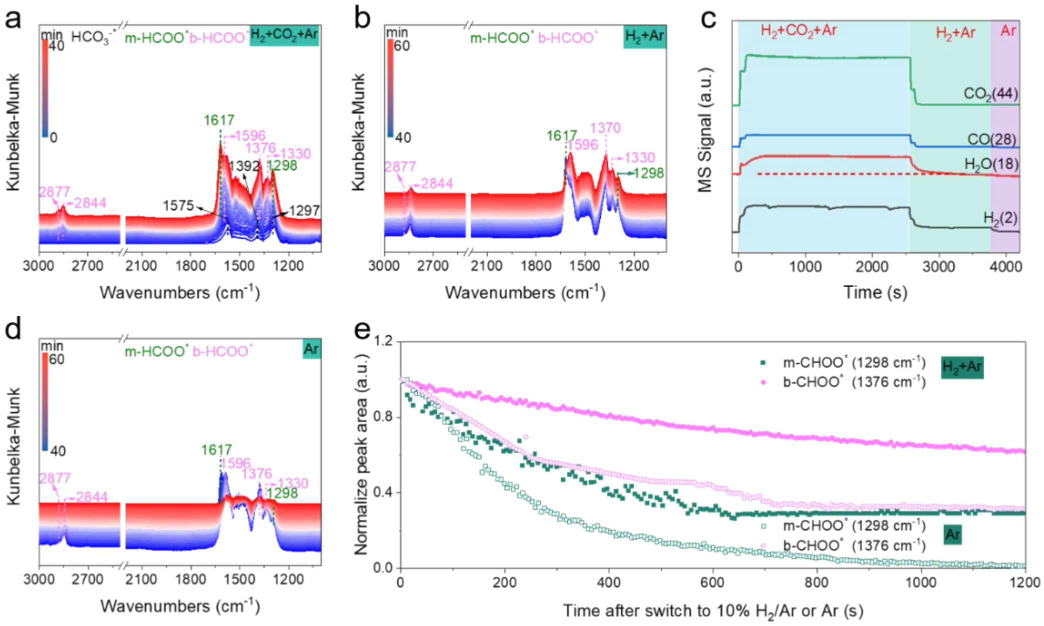

**Figure S7.** *In situ* time-resolved DRIFT spectra upon switch from (a) RWGS condition (t=0-40 min) to (b)10%$H_2$/Ar (t= 40-60 min) 225 °C. (c) The corresponding MS signals of gases in the effluent. (d) *In situ* time-resolved DRIFT spectra recorded after switch from the RWGS condition to Ar (t= 40-60 min). (e) The normalized peak area of surface monodentate formate (1298 cm$^{-1}$) and bidentate formate species (1376 cm$^{-1}$) as a function of time after the switch to 10%$H_2$/Ar or Ar (t=40-60 min).

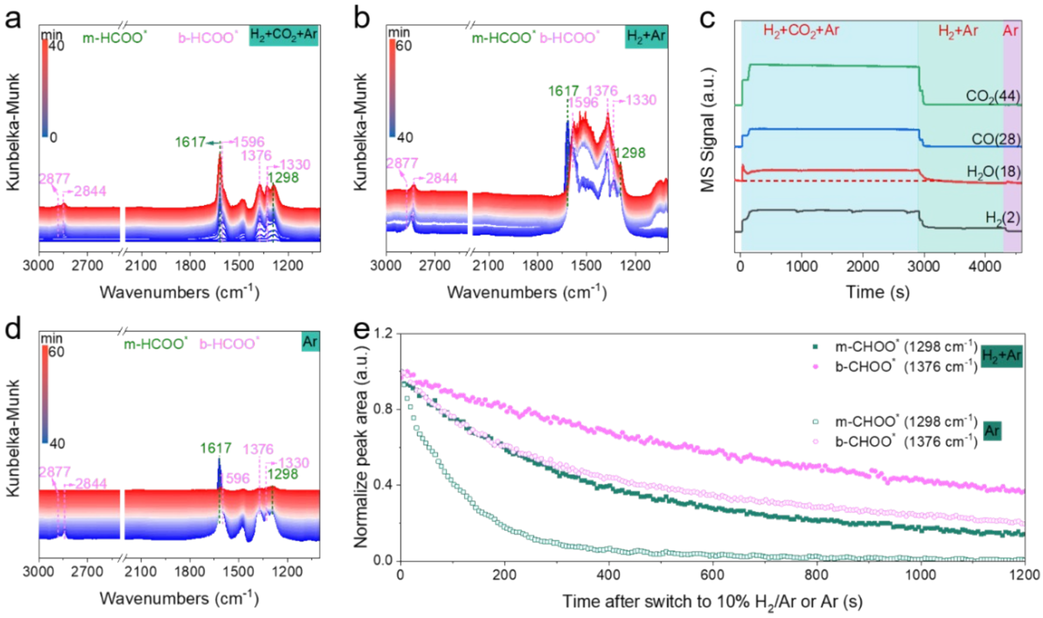

**Figure S8.** *In situ* time-resolved DRIFT spectra upon switch from (a) RWGS condition (t=0-40 min) to (b)10%$H_2$/Ar (t= 40-60 min) at 250 °C. (c) The corresponding MS signals of gases in the effluent. (d) *In situ* time-resolved DRIFT spectra recorded after switch from the RWGS condition to Ar (t= 40-60 min). (e) The normalized peak area of surface monodentate formate (1298 $cm^{-1}$) and bidentate formate species (1376 $cm^{-1}$) as a function of time after the switch to 10%$H_2$/Ar or Ar (t=40-60 min).

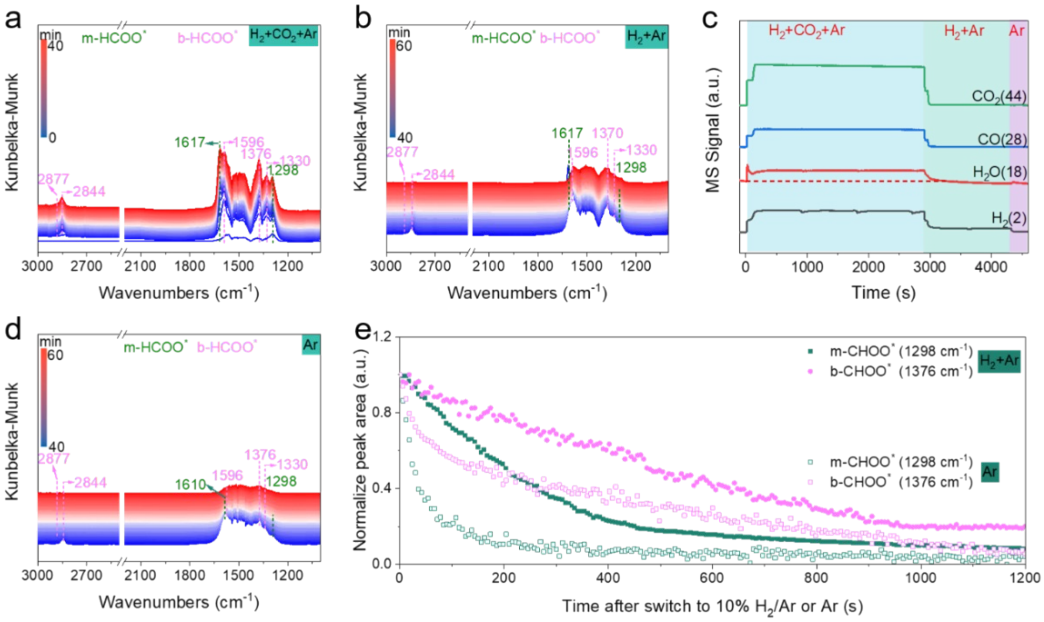

**Figure S9.** *In situ* time-resolved DRIFT spectra upon switch from (a) RWGS condition (t=0-40 min) to (b)10%$H_2$/Ar (t= 40-60 min) at 275 °C. (c) The corresponding MS signals of gases in the effluent. (d) *In situ* time-resolved DRIFT spectra recorded after switch from the RWGS condition to Ar (t= 40-60 min). (e) The normalized peak area of surface monodentate formate (1298 cm$^{-1}$) and bidentate formate species (1376 cm$^{-1}$) as a function of time after the switch to 10%$H_2$/Ar or Ar (t=40-60 min).

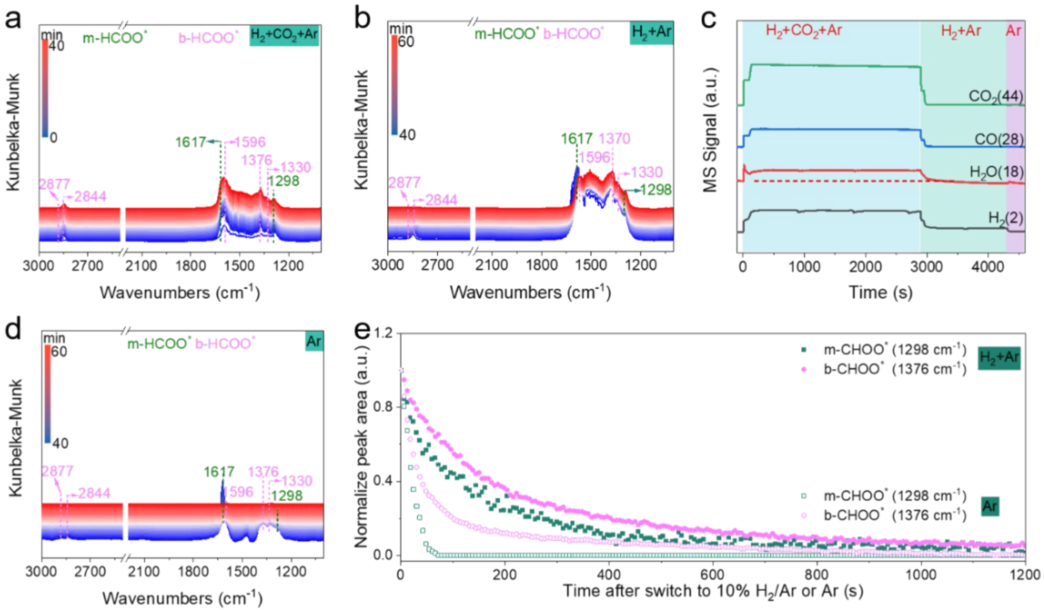

**Figure S10.** *In situ* time-resolved DRIFT spectra upon switch from (a) RWGS condition (t=0-40 min) to (b)10%$H_2$/Ar (t= 40-60 min) at 300 °C. (c) The corresponding MS signals of gases in the effluent. (d) *In situ* time-resolved DRIFT spectra recorded after switch from the RWGS condition to Ar (t= 40-60 min). (e) The normalized peak area of surface monodentate formate (1298 cm$^{-1}$) and bidentate formate species (1376 cm$^{-1}$) as a function of time after the switch to 10%$H_2$/Ar or Ar (t=40-60 min).

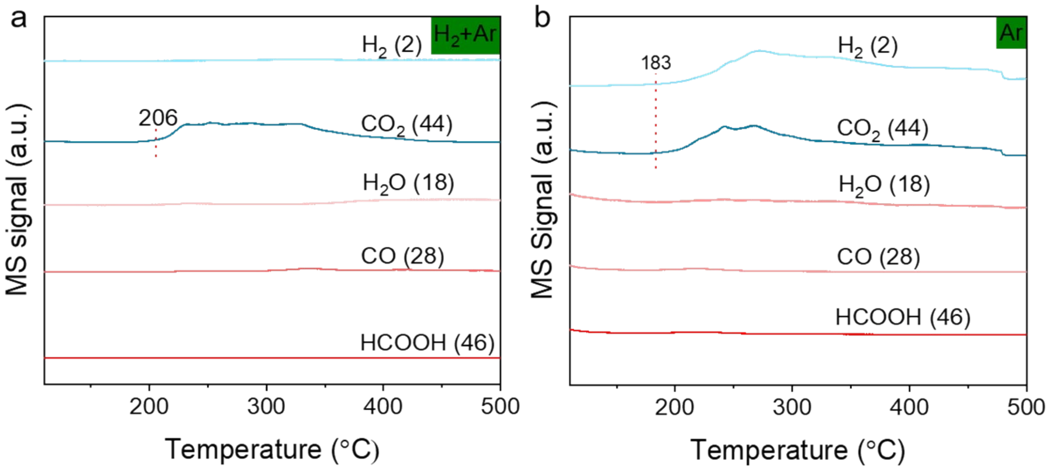

**Figure S11.** MS signals collected during HCOOH-TP of Cu/$CeO_2$ at ramping rate of 5 °C $min^{-1}$ in (a) 10%$H_2$/Ar and (b) Ar flowing.

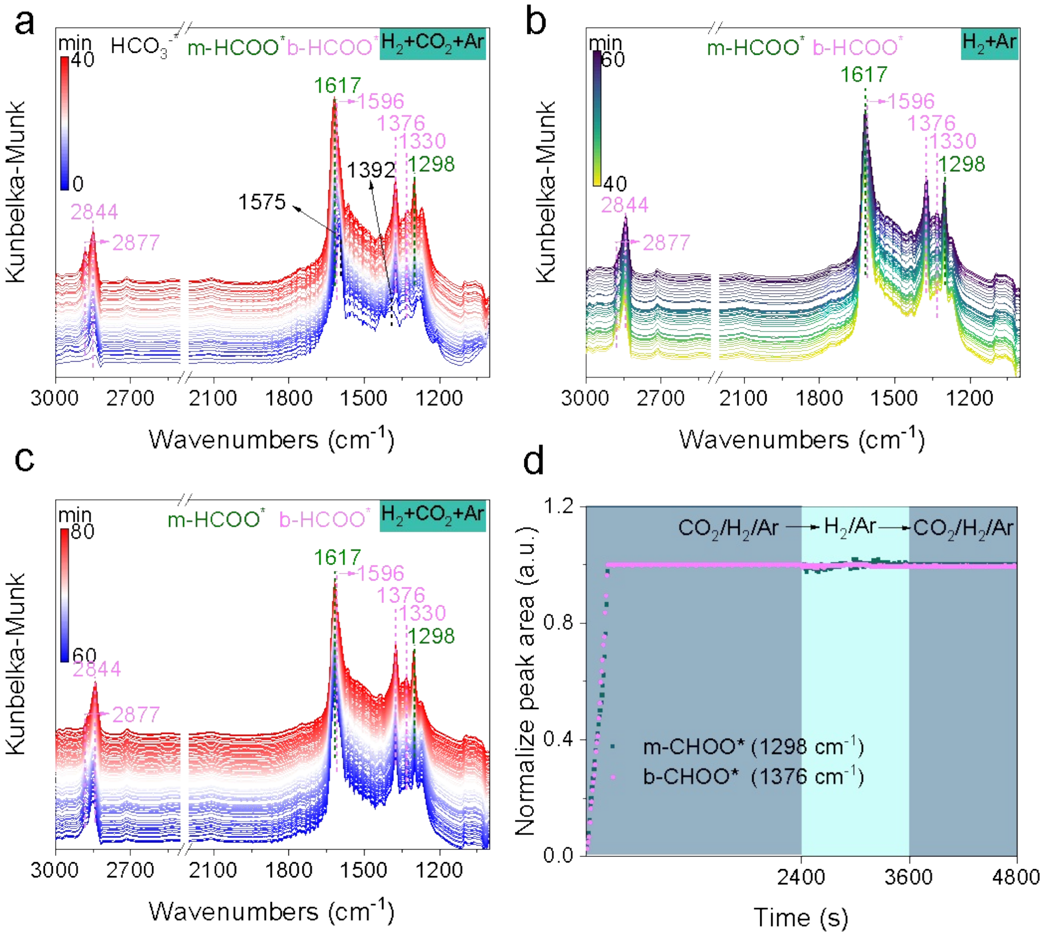

**Figure S12.** *In situ* time-resolved DRIFT spectra recorded under various conditions at 200 °C: (a) $CO_2/H_2/Ar$ (t=0-40 min) → (b) $H_2/Ar$ (t= 40-60 min) → (c) $CO_2/H_2/Ar$ (t=60-80 min). (d) The normalized peak area of surface monodentate formate (1298 cm$^{-1}$) and bidentate formate species (1376 cm$^{-1}$) as a function of time under various conditions.

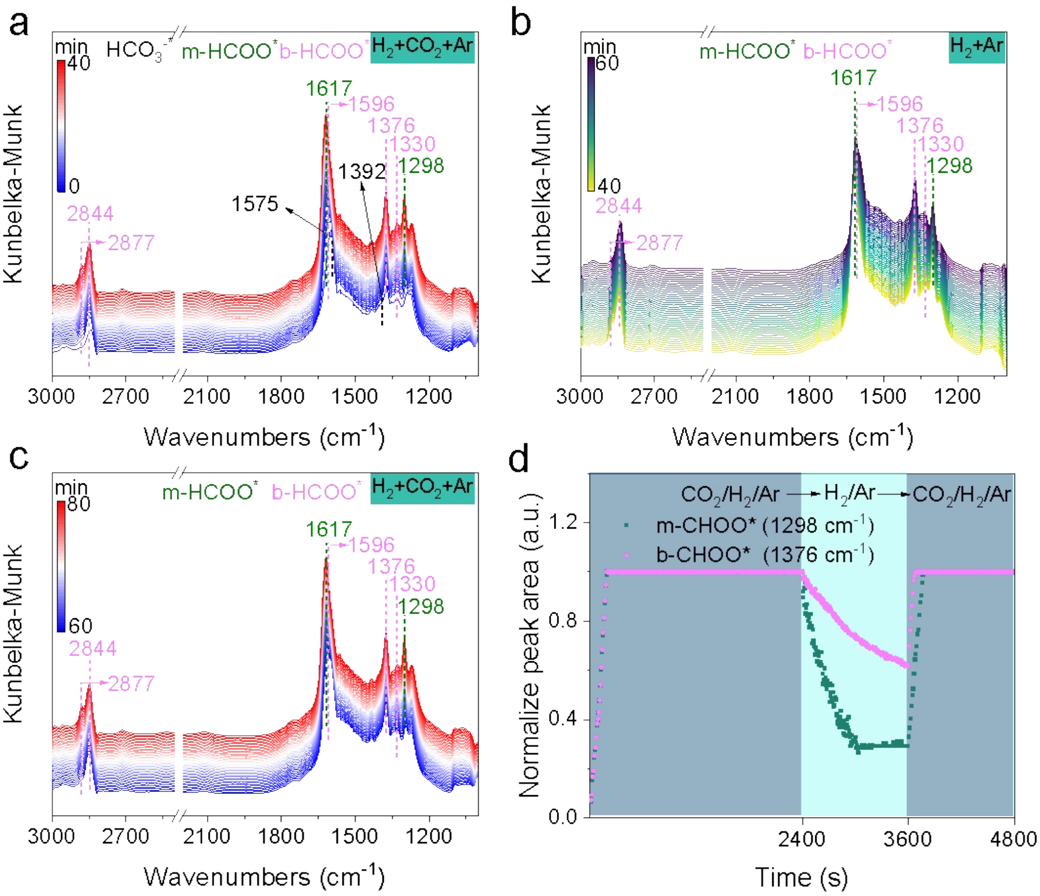

**Figure S13.** *In situ* time-resolved DRIFT spectra recorded under various conditions at 225 °C: (a) $CO_2/H_2/Ar$ (t=0-40 min) → (b) $H_2/Ar$ (t= 40-60 min) → (c) $CO_2/H_2/Ar$ (t=60-80 min). (d) The normalized peak area of surface monodentate formate (1298 $cm^{-1}$) and bidentate formate species (1376 $cm^{-1}$) as a function of time under various conditions.

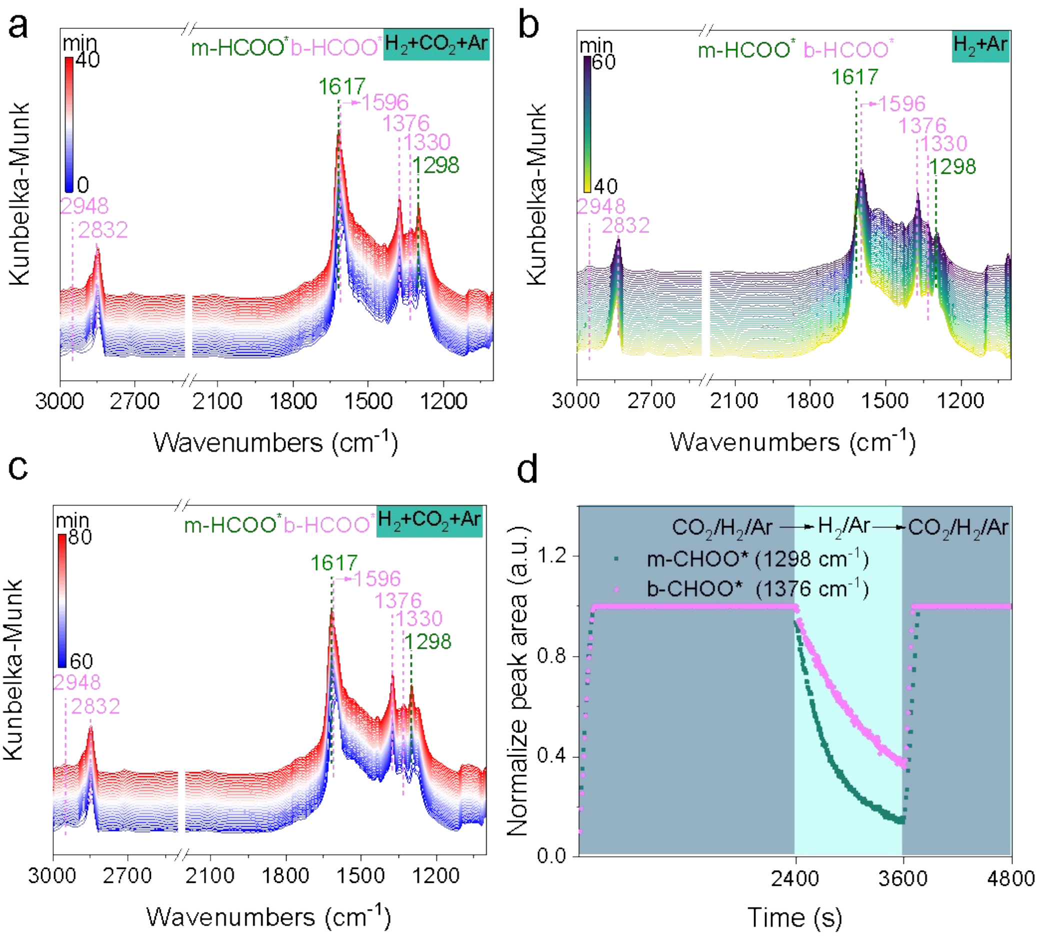

**Figure S14.** *In situ* time-resolved DRIFT spectra recorded under various conditions at 250 °C: (a) $CO_2/H_2/Ar$ (t=0-40 min) → (b) $H_2/Ar$ (t= 40-60 min) → (c) $CO_2/H_2/Ar$ (t=60-80 min). (d) The normalized peak area of surface monodentate formate (1298 $cm^{-1}$) and bidentate formate species (1376 $cm^{-1}$) as a function of time under various conditions.

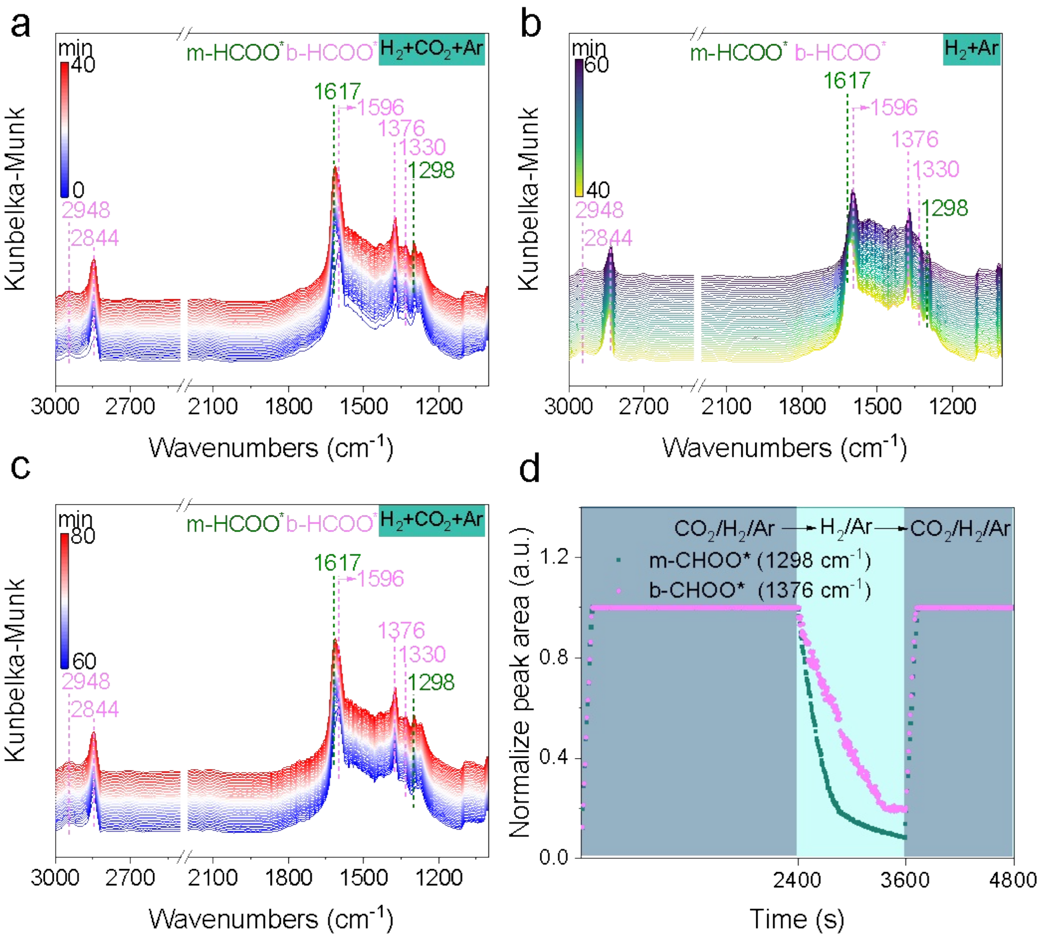

**Figure S15.** *In situ* time-resolved DRIFT spectra recorded under various conditions at 275 °C: (a) $CO_2/H_2/Ar$ (t=0-40 min) → (b) $H_2/Ar$ (t= 40-60 min) → (c) $CO_2/H_2/Ar$ (t=60-80 min). (d) The normalized peak area of surface monodentate formate (1298 cm$^{-1}$) and bidentate formate species (1376 cm$^{-1}$) as a function of time under various conditions.

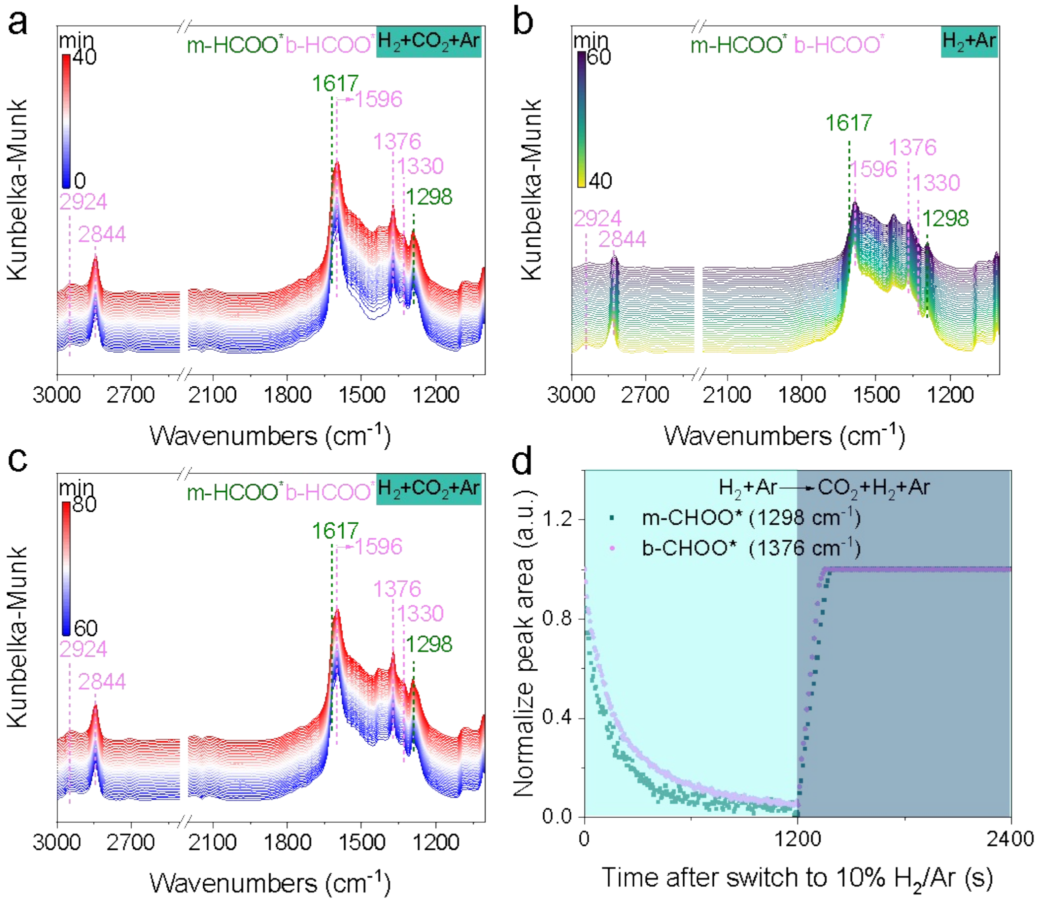

**Figure S16.** *In situ* time-resolved DRIFT spectra recorded under various conditions at 300 °C: (a) $CO_2/H_2/Ar$ (t=0-40 min) → (b) $H_2/Ar$ (t= 40-60 min) → (c) $CO_2/H_2/Ar$ (t=60-80 min). (d) The normalized peak area of surface monodentate formate (1298 cm$^{-1}$) and bidentate formate species (1376 cm$^{-1}$) as a function of time under various conditions.

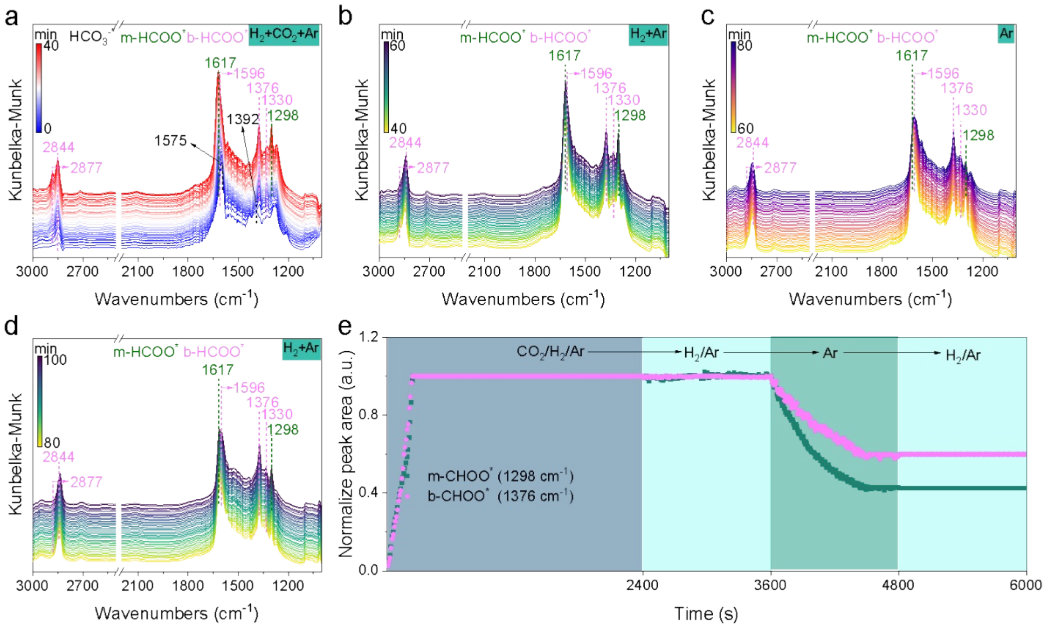

**Figure S17.** *In situ* time-resolved DRIFT spectra recorded under various conditions at 200 °C: (a) $CO_2/H_2/Ar$ (t=0-40 min) → (b) $H_2/Ar$ (t= 40-60 min) → (c) Ar (t=60-80 min) → (d) $H_2/Ar$ (t=80-100 min). (e) The normalized peak area of surface monodentate formate (1298 $cm^{-1}$) and bidentate formate species (1376 $cm^{-1}$) as a function of time under various conditions.

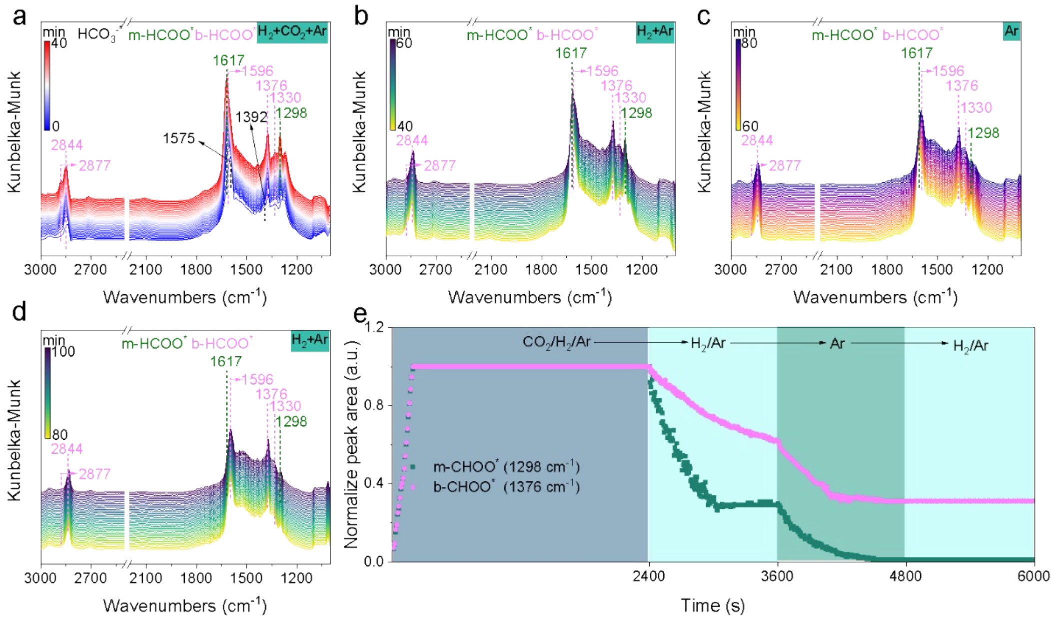

**Figure S18.** *In situ* time-resolved DRIFT spectra recorded under various conditions at 225 °C: (a) $CO_2/H_2/Ar$ (t=0-40 min) → (b) $H_2/Ar$ (t= 40-60 min) → (c) Ar (t=60-80 min) → (d) $H_2/Ar$ (t=80-100 min). (e) The normalized peak area of surface monodentate formate (1298 cm$^{-1}$) and bidentate formate species (1376 cm$^{-1}$) as a function of time under various conditions.

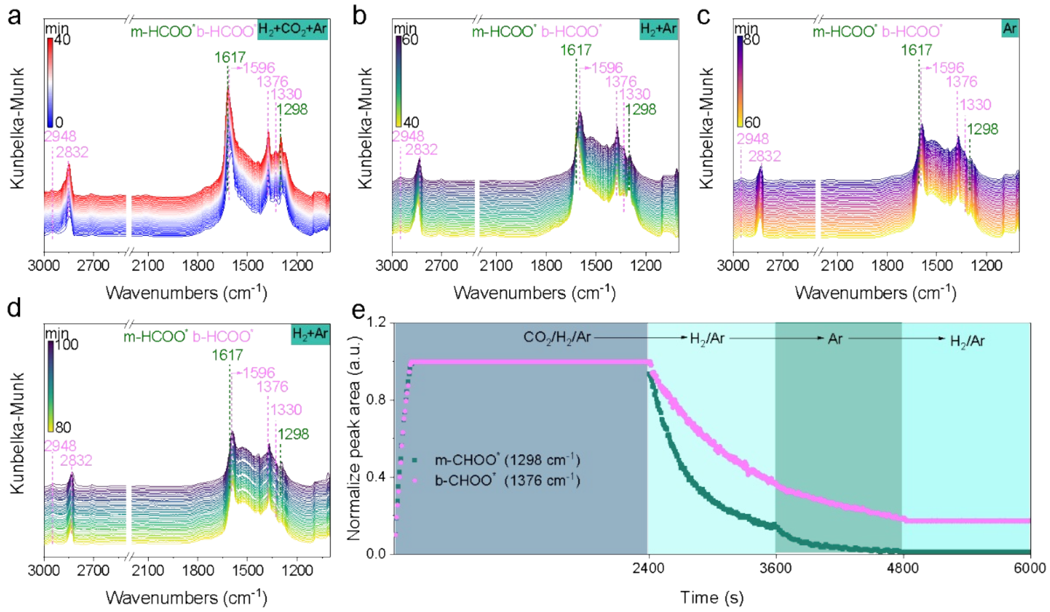

**Figure S19.** *In situ* time-resolved DRIFT spectra recorded under various conditions at 250 °C: (a) $CO_2/H_2/Ar$ (t=0-40 min) → (b) $H_2/Ar$ (t= 40-60 min) → (c) Ar (t=60-80 min) → (d) $H_2/Ar$ (t=80-100 min). (e) The normalized peak area of surface monodentate formate (1298 cm$^{-1}$) and bidentate formate species (1376 cm$^{-1}$) as a function of time under various conditions.

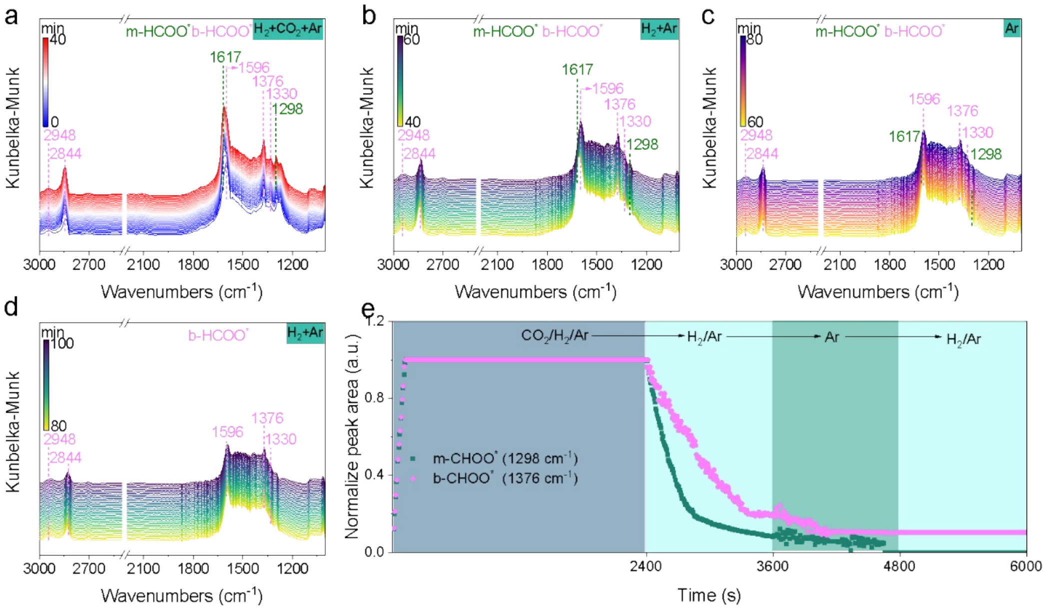

**Figure S20.** *In situ* time-resolved DRIFT spectra recorded under various conditions at 275 °C: (a) $CO_2/H_2/Ar$ (t=0-40 min) → (b) $H_2/Ar$ (t= 40-60 min) → (c) Ar (t=60-80 min) → (d) $H_2/Ar$ (t=80-100 min). (e) The normalized peak area of surface monodentate formate (1298 $cm^{-1}$) and bidentate formate species (1376 $cm^{-1}$) as a function of time under various conditions.

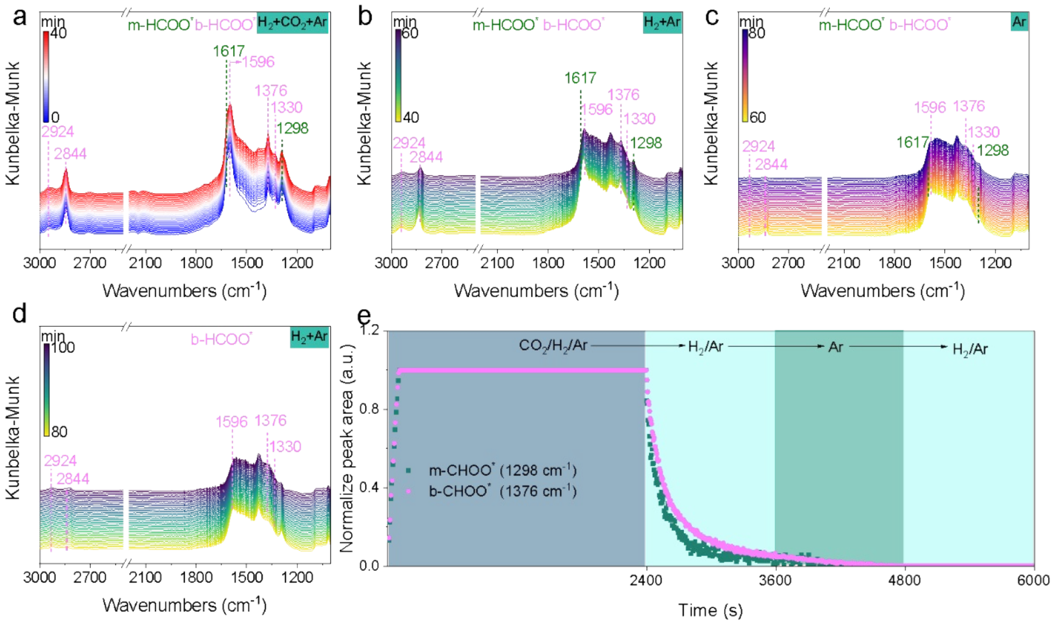

**Figure S21.** *In situ* time-resolved DRIFT spectra recorded under various conditions at 300 °C: (a) $CO_2/H_2/Ar$ (t=0-40 min) → (b) $H_2/Ar$ (t= 40-60 min) → (c) Ar (t=60-80 min) → (d) $H_2/Ar$ (t=80-100 min). (e) The normalized peak area of surface monodentate formate (1298 $cm^{-1}$) and bidentate formate species (1376 $cm^{-1}$) as a function of time under various conditions.

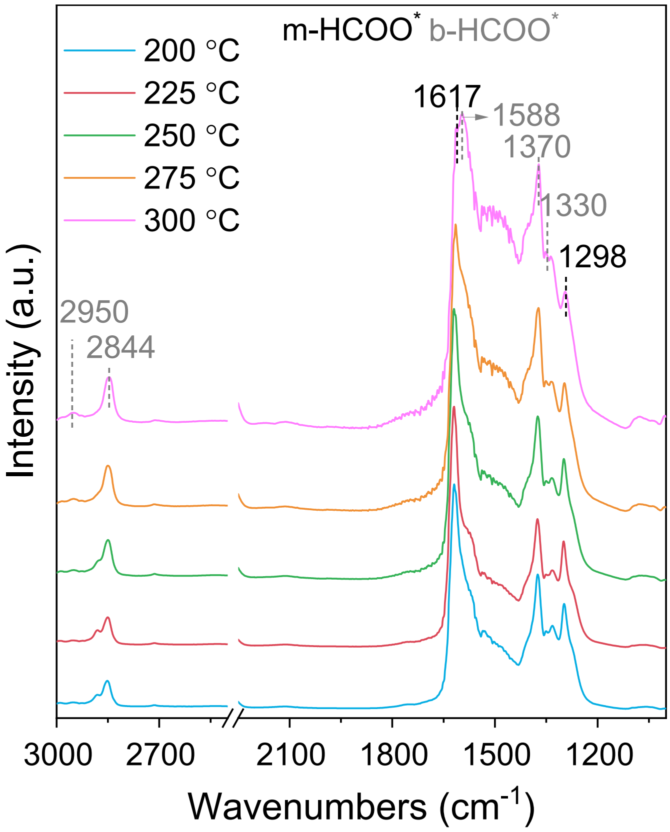

**Figure S22.** *In situ* DRIFT spectra continuously collected in same sample during RWGS condition at different temperatures.

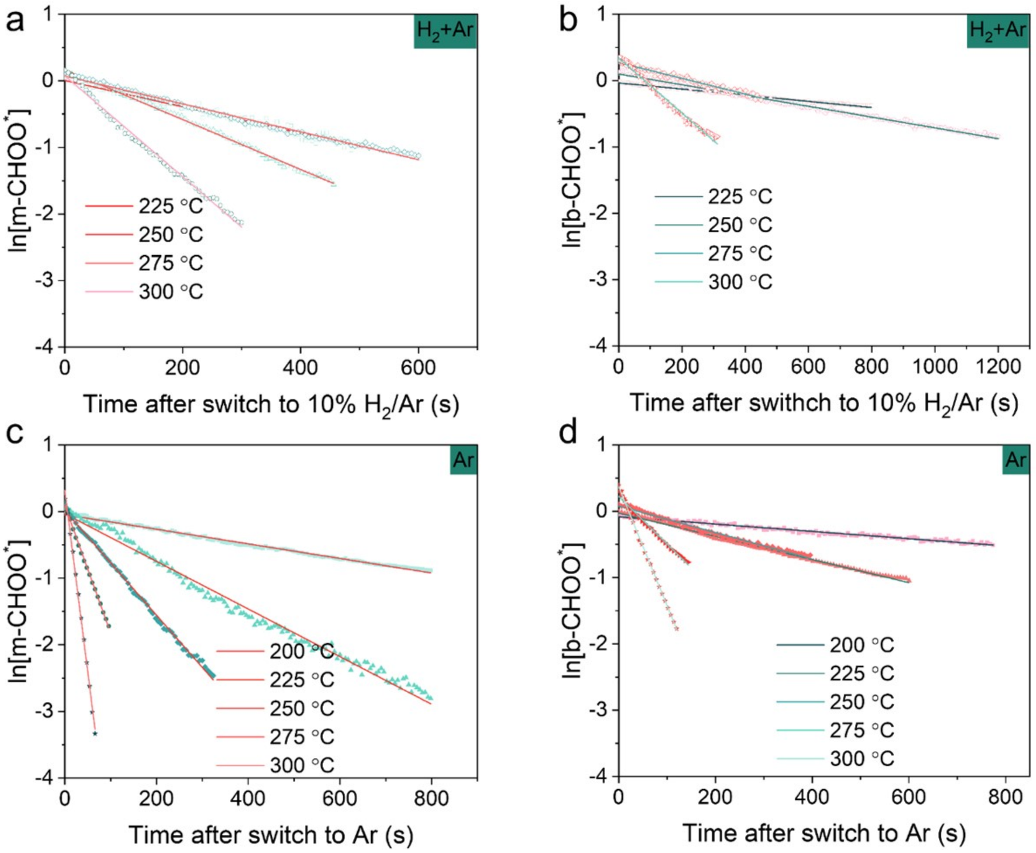

**Figure S23.** Semilogarithmic plots of evolutions of relative intensities of surface (a) monodentate formate and (b) bidentate formate species as a function of time after switch to 10%$H_2$/Ar at different temperatures. Semilogarithmic plots of evolutions of relative intensities of surface (c) monodentate formate and (d) bidentate formate species as a function of time after switch to Ar at different temperatures.

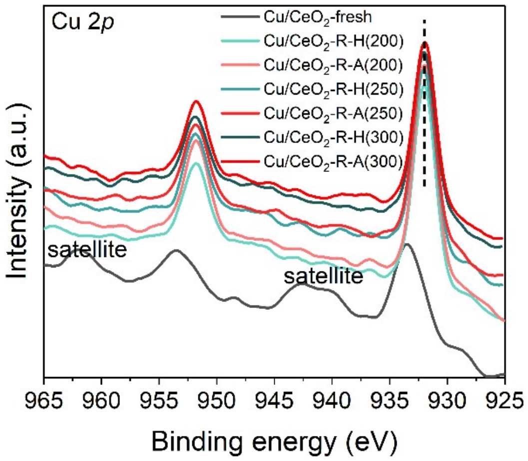

**Figure S24.** Quasi *in situ* XPS spectra of Cu 2*p* for the fresh Cu/$CeO_2$ catalyst and the reaction-treated Cu/$CeO_2$ catalyst with switching to a 10%$H_2$/Ar or Ar flow at different temperature.

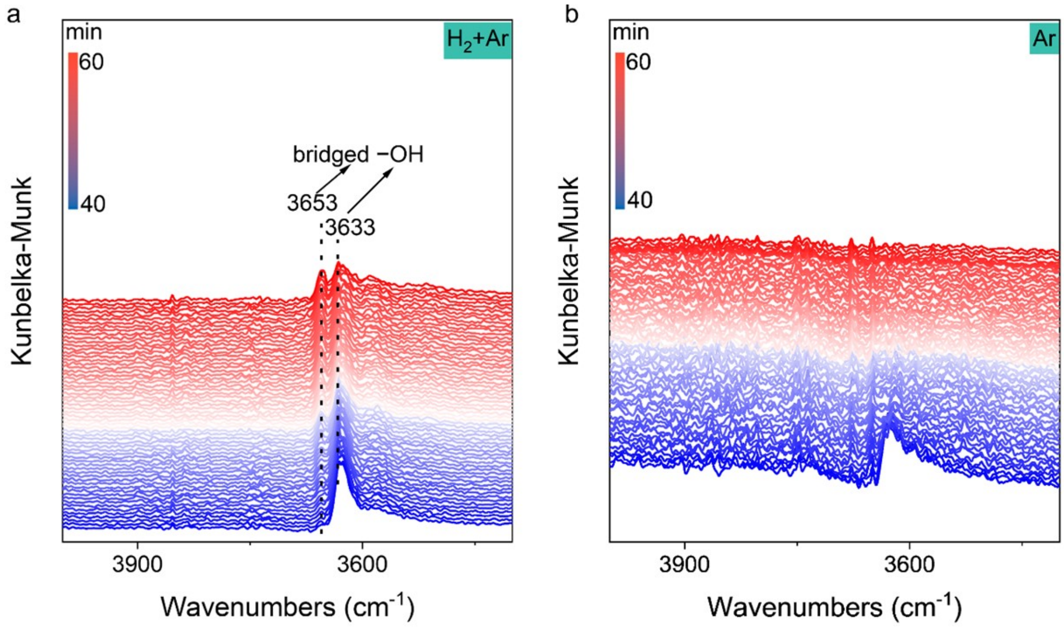

**Figure S25.** *Operando* DRIFT spectra of Cu/$CeO_2$ under a (a) 10%$H_2$/Ar flow and (b) Ar flow at 225 °C showing the hydroxyl region (t=40-60 min).

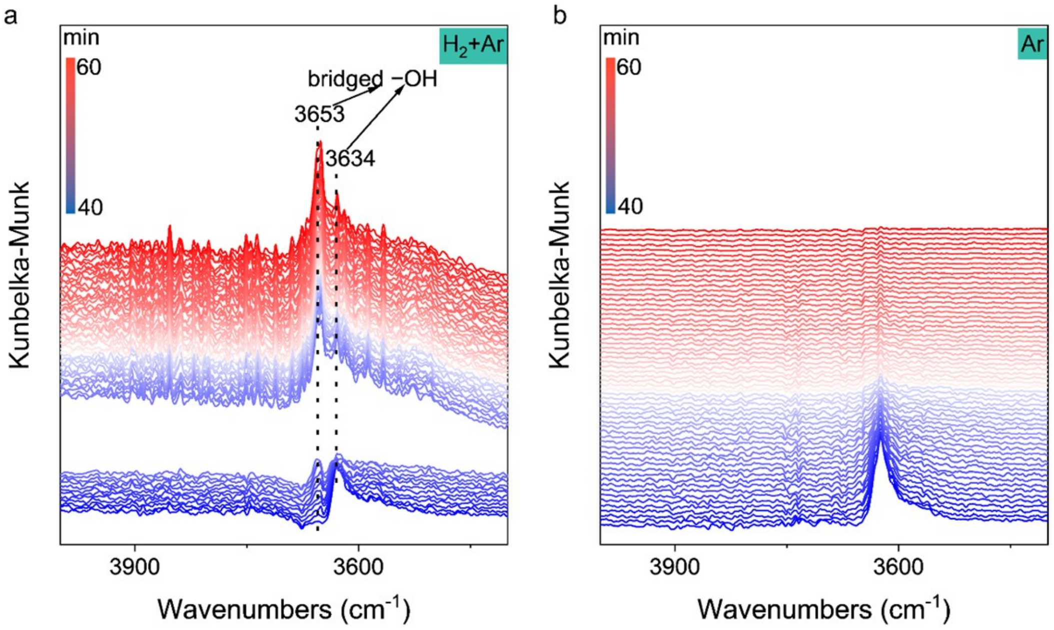

**Figure S26.** *Operando* DRIFT spectra of Cu/$CeO_2$ under a (a) 10%$H_2$/Ar flow and (b) Ar flow at 250 °C showing the hydroxyl region (t=40-60 min).

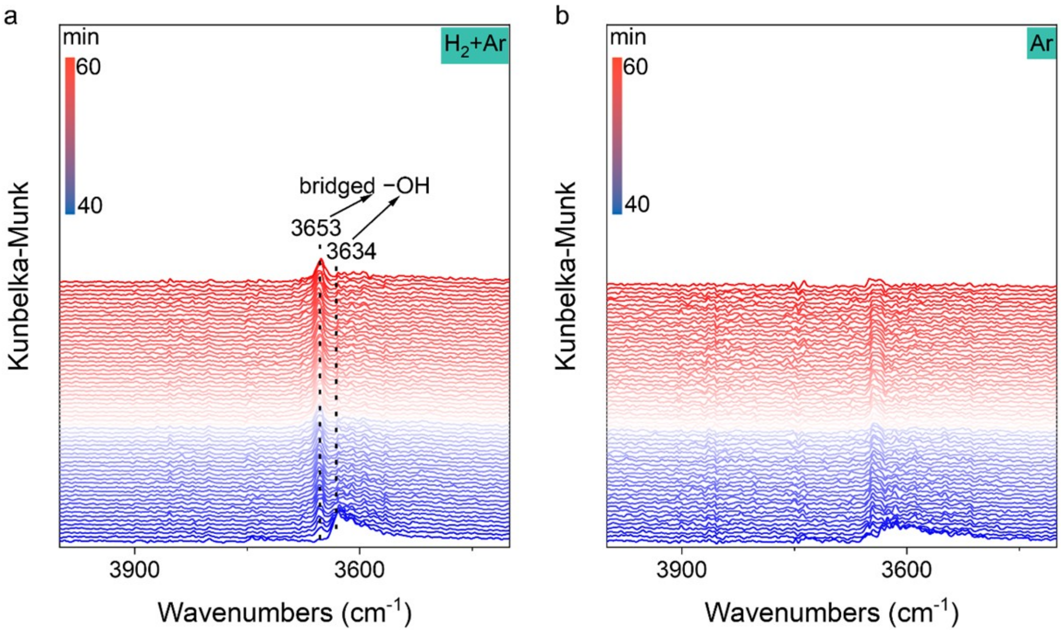

**Figure S27.** *Operando* DRIFT spectra of Cu/CeO$_2$ under a (a) 10%H$_2$/Ar flow and (b) Ar flow at 275 °C showing the hydroxyl region (t=40-60 min).

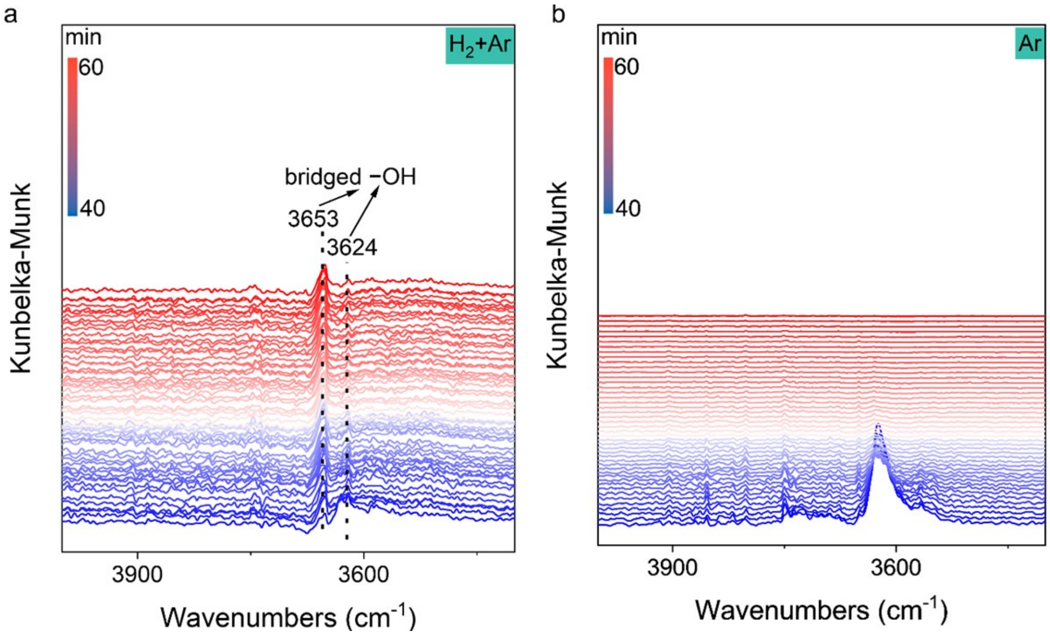

**Figure S28.** *Operando* DRIFT spectra of Cu/$CeO_2$ under a (a) 10%$H_2$/Ar flow and (b) Ar flow at 300 °C showing the hydroxyl region (t=40-60 min).

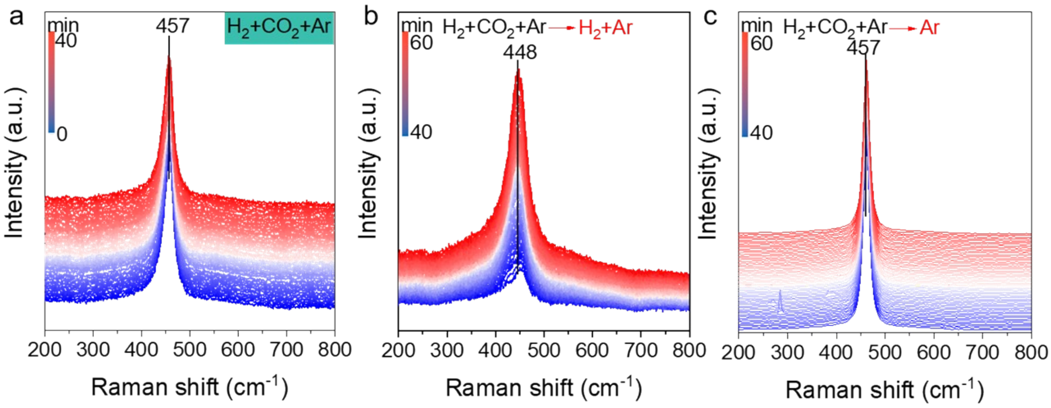

**Figure S29.** *In situ* time-resolved Raman spectra upon switch from (a) RWGS condition (t=0-40 min) to either (b) 10%$H_2$/Ar (t= 40-60 min) or (c) Ar (t= 40-60 min) at 200 °C.

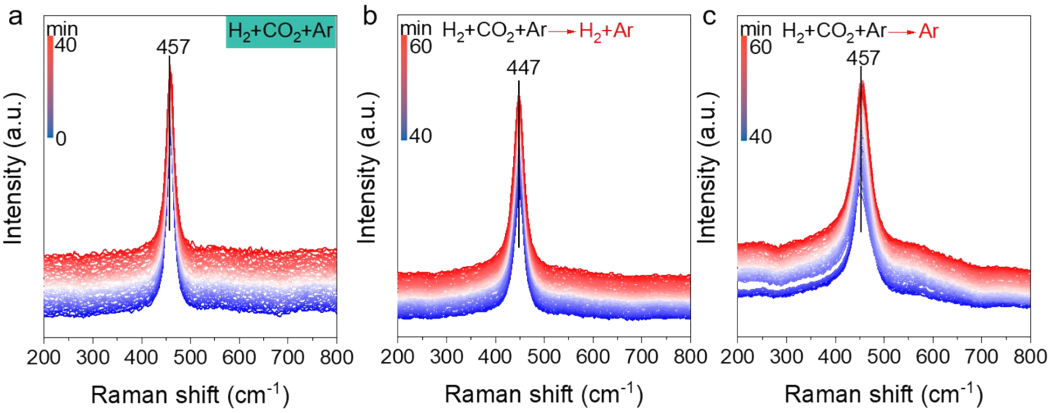

**Figure S30.** *In situ* time-resolved Raman spectra upon switch from (a) RWGS condition (t=0-40 min) to either (b) 10%$H_2$/Ar (t= 40-60 min) or (c) Ar (t= 40-60 min) at 225 °C.

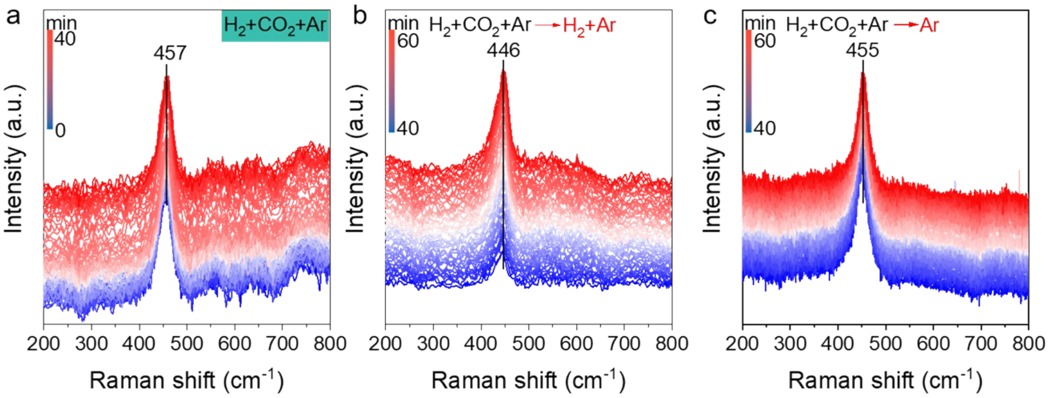

**Figure S31.** *In situ* time-resolved Raman spectra upon switch from (a) RWGS condition (t=0-40 min) to either (b) 10%$H_2$/Ar (t= 40-60 min) or (c) Ar (t= 40-60 min) at 250 °C.

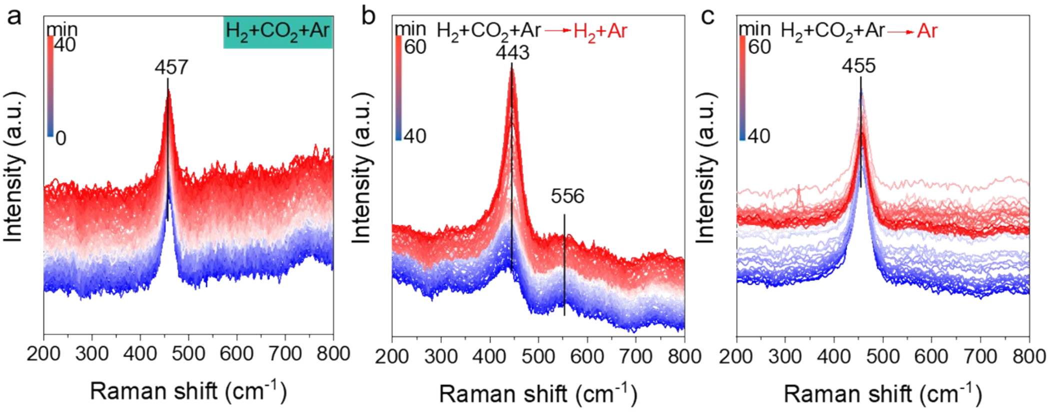

**Figure S32.** *In situ* time-resolved Raman spectra upon switch from (a) RWGS condition (t=0-40 min) to either (b) 10%$H_2$/Ar (t= 40-60 min) or (c) Ar (t= 40-60 min) at 275 °C.

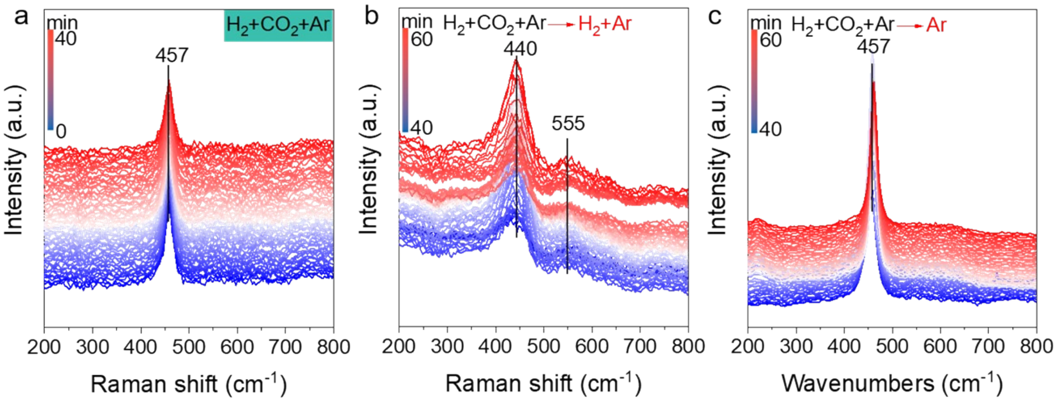

**Figure S33.** *In situ* time-resolved Raman spectra upon switch from (a) RWGS condition (t=0-40 min) to either (b) 10%$H_2$/Ar (t= 40-60 min) or (c) Ar (t= 40-60 min) at 300 °C.

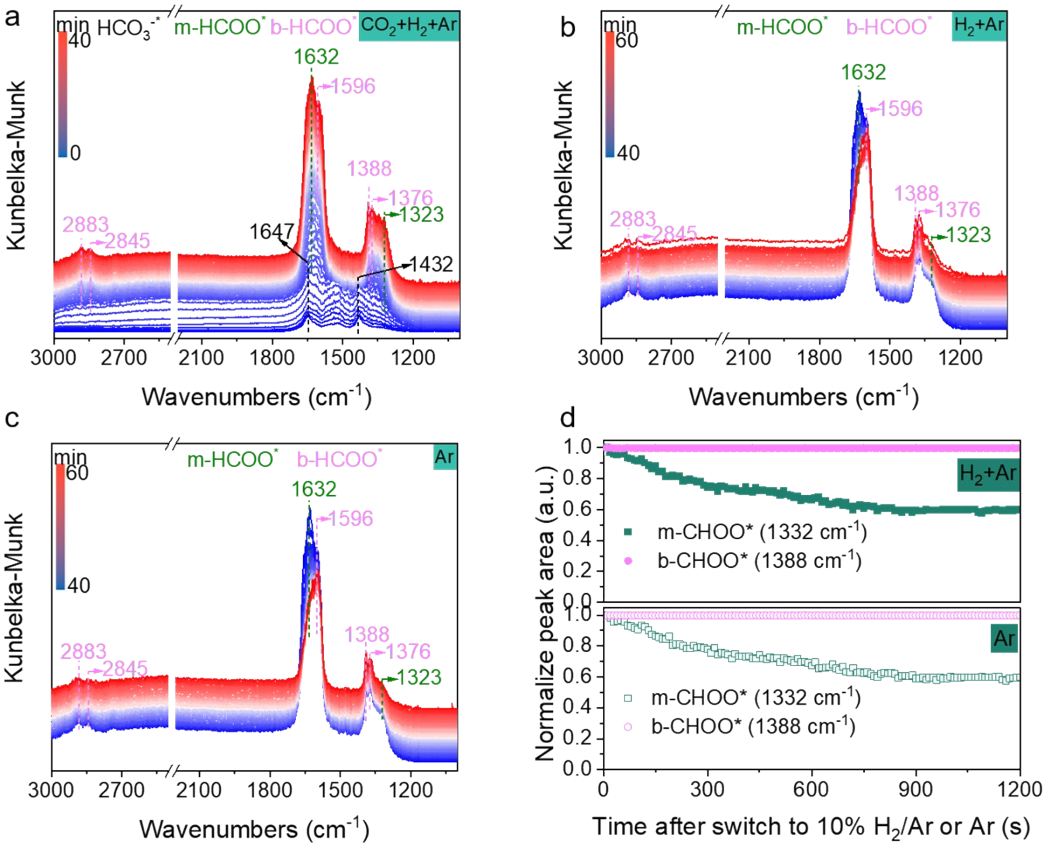

**Figure S34.** *In situ* time-resolved DRIFT spectra upon switch from (a) RWGS condition (t=0-40 min) to (b) 10%$H_2$/Ar (t= 40-60 min) or (c) Ar (t= 40-60 min) for Cu/$Al_2O_3$ at 200 °C. (d) The normalized peak area of surface monodentate formate (1332 $cm^{-1}$) and bidentate formate species (1388 $cm^{-1}$) as a function of time after the switch to 10%$H_2$/Ar or Ar (t=40-60 min).

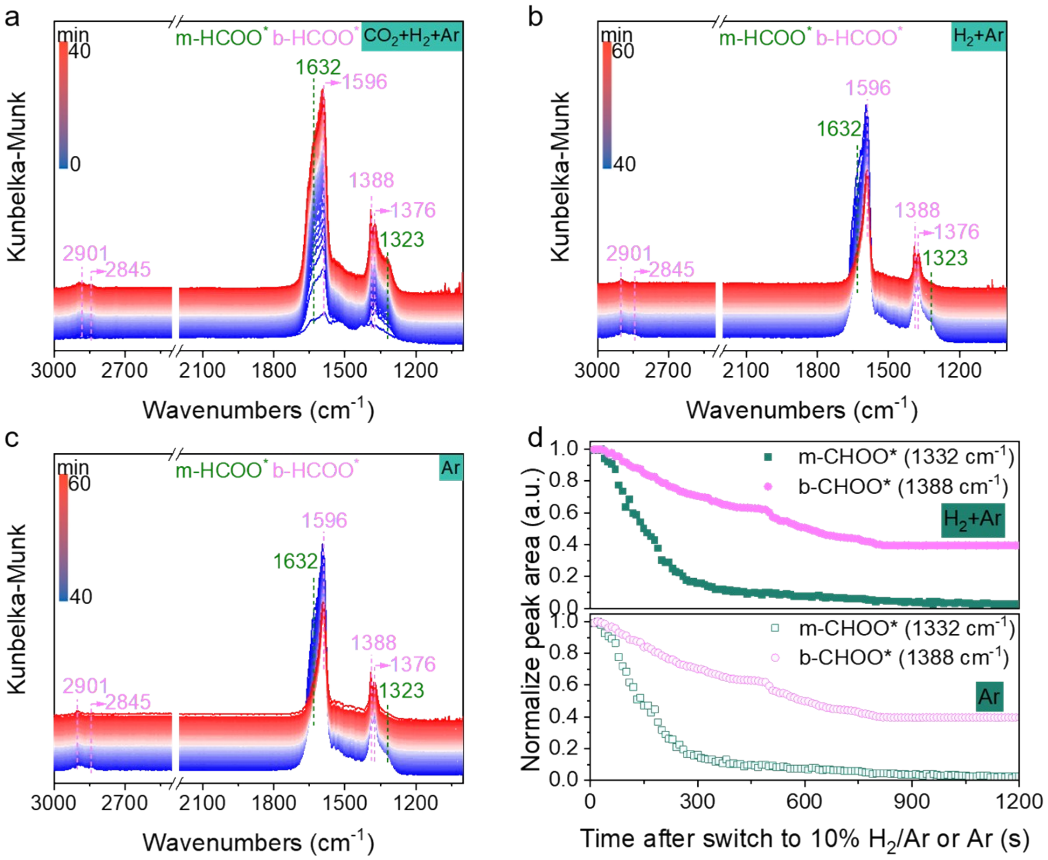

**Figure S35.** *In situ* time-resolved DRIFT spectra upon switch from (a) RWGS condition (t=0-40 min) to (b) 10%$H_2$/Ar (t= 40-60 min) or (c) Ar (t= 40-60 min) for Cu/$Al_2O_3$ at 250 °C. (d) The normalized peak area of surface monodentate formate (1332 cm$^{-1}$) and bidentate formate species (1388 cm$^{-1}$) as a function of time after the switch to 10%$H_2$/Ar or Ar (t=40-60 min).

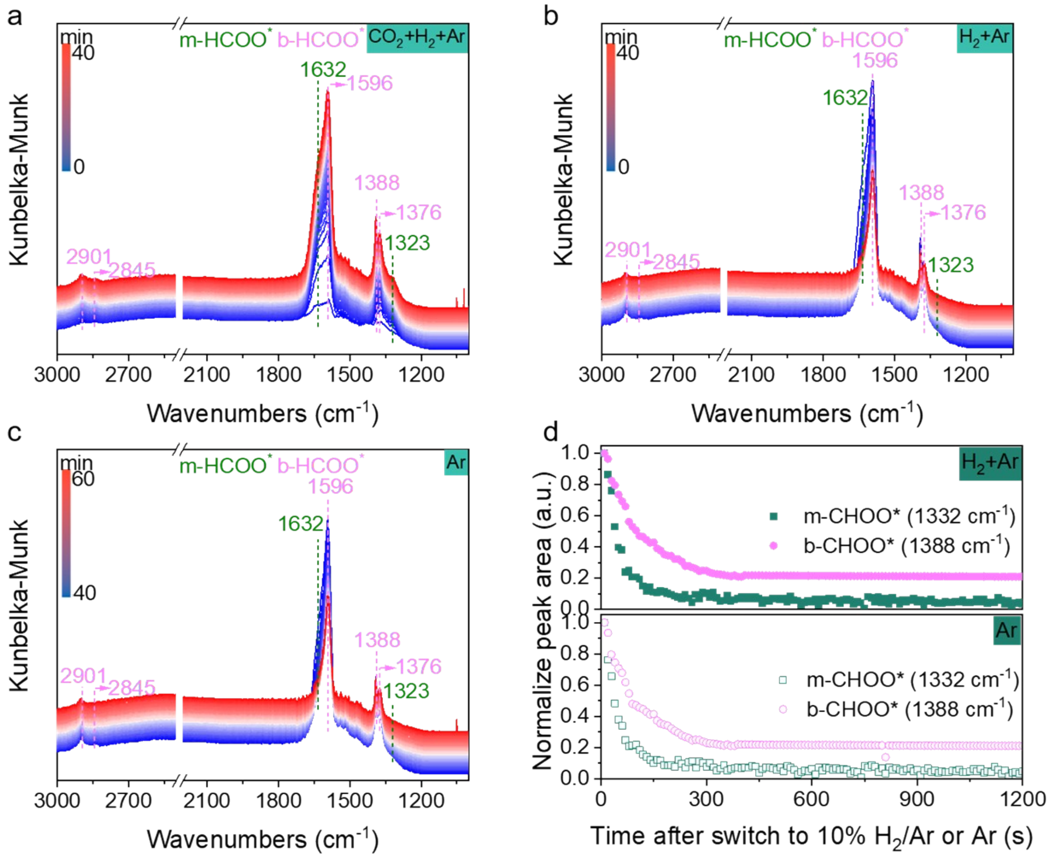

**Figure S36.** *In situ* time-resolved DRIFT spectra upon switch from (a) RWGS condition (t=0-40 min) to (b) 10%$H_2$/Ar (t= 40-60 min) or (c) Ar (t= 40-60 min) for $Cu/Al_2O_3$ at 300 °C. (d) The normalized peak area of surface monodentate formate (1332 cm$^{-1}$) and bidentate formate species (1388 cm$^{-1}$) as a function of time after the switch to 10%$H_2$/Ar or Ar (t=40-60 min).

**Table S1.** Residence time distribution of various gases in the *in situ* reaction system with the low void-volume reaction cell.

| Gas | $t_{m,r}$ ($\sigma$) (s) | $\tau_{p,r}$ (s) | $\tau_{p,b}$ (s) | $t_{m,1}$ (s) | $t_{m,2}$ (s) |
|---|---|---|---|---|---|
| Ar | 13.7 (3.2) | 6.8 | 5.5 | 1.9 | 5.0 |
| $H_2$ | 13.2 (2.8) | 7.0 | 5.8 | 1.5 | 4.7 |
| $CO_2$ | 13.6 (3.1) | 6.9 | 5.8 | 2.0 | 4.7 |
| Average | 13.5 | 6.9 | 5.7 | 1.8 | 4.8 |

$t_{m,r}$ = mean residence time of pulse gas to reach MS detector (via in situ reaction cell), $\sigma$ = standard deviation, $\tau_{p,r}$ = space time for a plug flow reactor: tubing line before in situ reaction cell, $\tau_{p,b}$ = space time for a plug flow reactor: tubing line bypassing *in situ* reaction cell, $t_{m,1}$ = mean residence time of pulse gas through *in situ* reactor based on an ideal CSTR, $t_{m,2}$ = mean residence time of pulse gas in mass spectrometer before reaching detector based on an ideal CSTR. Experimental conditions: He carrier 50 mL min$^{-1}$, 100 μL gas pulse, 1 bar, 25 °C.

**Table S2**. The RWGS activity with different reactor over Cu/$CeO_2$ at different temperatures.

| T (°C) | GHSV ($mL\ g^{-1}\ h^{-1}$) | $X_{CO2}$ (%) | CO rate ($\times 10^{-3}$ mmol $g_{cat}^{-1}$ $s^{-1}$)[a] | CO rate ($\times 10^{-3}$ mmol $g_{cat}^{-1}$ $s^{-1}$)[b] |
|---|---|---|---|---|
| 200 | 60000 | 2.4 | 1.77±0.10 | 1.70±0.15 |
| 225 | 60000 | 5.0 | 3.73±0.1 | 3.60±0.10 |
| 250 | 60000 | 8.5 | 6.34±0.2 | 6.50±0.25 |
| 275 | 120000 | 8.0 | 11.95±0.4 | 12.00±0.30 |
| 300 | 240000 | 7.1 | 21.15±0.3 | 22.00±0.30 |

[a] The activity measured by fixed-bed reactor.

[b] The activity measured by low void-volume cell.

**Table S3.** Assignments of observed bands on $CeO_2$-supported catalysts during *in situ* DRIFTS experiments.

| Species assignment with ceria support | Wavenumbers ($cm^{-1}$) | Literature |
|---|---|---|
| Monodentate formate | 2945, 2830, 2711, 1595, 1276 | [7] |
| | 2924, 2833, 1611, 1295 | [5] |
| Bidentate formate | 2924, 2833, 1563, 1354 | [5] |
| | 2945, 2838, 2712, 1585, 1369, 1334 | [8] |
| | 2947, 2845, 1373, 1356 | [9] |
| | 2940, 2845, 1558-1590, 1330-1370 | [10] |

**Table S4.** The raw and initial intensities of surface monodentate formate (m-CHOO*) and bidentate formate (b-CHOO*) species according to the *in situ* temperature-dependent DRIFTS obtained from Figure S12.

| T (°C) | Raw intensity of m-CHOO* (a. u.) | Raw intensity of b-CHOO* (a. u.) | Initial intensity of m-CHOO* (a. u.)[a] | Initial intensity of b-CHOO* (a. u.)[a] |
|---|---|---|---|---|
| 200 | 8.90 | 8.81 | 1.00 | 0.99 |
| 225 | 9.34 | 8.81 | 1.05 | 0.99 |
| 250 | 9.88 | 9.97 | 1.11 | 1.12 |
| 275 | 10.41 | 12.02 | 1.17 | 1.35 |
| 300 | 10.77 | 14.77 | 1.21 | 1.66 |

[a] The initial intensities are determined according to the *in situ* temperature-dependent DRIFTS in a $CO_2/H_2$ flow and normalized against the values of m-CHOO$^*$ obtained at 200 °C.

**Table S5**. The rate constants of monodentate formate (m-CHOO$^*$) and bidentate formate (b-CHOO$^*$) data derived from switching (45%$CO_2$/45%$H_2$/10%Ar to →10% $H_2$/Ar (or Ar)) over Cu/$CeO_2$ at different temperatures.[a]

| T | 10%$H_2$/Ar | | Ar | |
|---|---|---|---|---|
| (°C) | $k^d_{m\text{-}CHOO*}$ | $k^d_{b\text{-}CHOO*}$ | $k^d_{m\text{-}CHOO*}$ | $k^d_{b\text{-}CHOO*}$ |
| 200 | - | - | 0.0011±0.00002 | 0.0006±0.00004 |
| 225 | 0.0020±0.00004 | 0.0005±0.00001 | 0.0036±0.00003 | 0.0018±0.00001 |
| 250 | 0.0021±0.00002 | 0.0008±0.00001 | 0.0079±0.00006 | 0.0020±0.00003 |
| 275 | 0.0038±0.00002 | 0.0012±0.0002 | 0.0192±0.00022 | 0.0072±0.00013 |
| 300 | 0.0076±0.00009 | 0.0039±0.00007 | 0.0543±0.00088 | 0.0179±0.00014 |

[a] $k^d$ represents decomposition rate constants.

**Table S6**. Surface compositions of $Cu/CeO_2$ after a series of treatments based on quasi *in situ* XPS.

| Samples | Cu/Ce | $Cu^0$ (%) | $Cu^+$ (%) | $Ce^{3+}/(Ce^{3+}+Ce^{4+})$ (%) |
|---|---|---|---|---|
| $Cu/CeO_2$-R-A(200) | 0.36 | 85.2 | 14.8 | 19.2 |
| $Cu/CeO_2$-R-A(250) | 0.39 | 85.8 | 14.2 | 24.8 |
| $Cu/CeO_2$-R-A(300) | 0.37 | 85.4 | 14.6 | 33.1 |
| $Cu/CeO_2$-R-H(200) | 0.38 | 85.0 | 15.0 | 26.7 |
| $Cu/CeO_2$-R-H(250) | 0.38 | 85.5 | 14.5 | 36.4 |
| $Cu/CeO_2$-R-H(300) | 0.35 | 85.4 | 14.6 | 42.0 |

## References

1. B. S. Patil, P. D. Srinivasan, E. Atchison, H. Zhu and J. J. Bravo-Suárez, *React. Chem. Eng.*, 2019, **4**, 667-678.
2. P. D. Srinivasan, S. R. Nitz, K. J. Stephens, E. Atchison and J. J. Bravo-Suarez, *Appl. Catal., A*, 2018, **561**, 7-18.
3. G. Jacobs, P. M. Patterson, U. M. Graham, D. E. Sparks and B. H. Davis, *Appl. Catal., A*, 2004, **269**, 63-73.
4. T. Shido and Y. Iwasawa, *J. Catal.*, 1992, **136**, 493-503.
5. J. Zhu, Y. Su, J. Chai, V. Muravev, N. Kosinov and E. J. M. Hensen, *ACS Catal.*, 2020, **10**, 11532-11544.
6. N. C. Nelson, M.-T. Nguyen, V.-A. Glezakou, R. Rousseau and J. Szanyi, *Nat. Catal.*, 2019, **2**, 916-924.
7. J. Vecchietti, A. Bonivardi, W. Xu, D. Stacchiola, J. J. Delgado, M. Calatayud and S. E. Collins, *ACS Catal.*, 2014, **4**, 2088-2096.
8. M. Ziemba, J. Weyel and C. Hess, *Appl. Catal., B*, 2022, **301**, 120825.
9. D. Vovchok, C. Zhang, S. Hwang, L. Jiao, F. Zhang, Z. Liu, S. D. Senanayake and J. A. Rodriguez, *ACS Catal.*, 2020, **10**, 10216-10228.
10. A. Hornés, P. Bera, A. L. Cámara, D. Gamarra, G. Munuera and A. Martínez-Arias, *J. Catal.*, 2009, **268**, 367-375.